Hybrid Silver Nanowire–CMC Aerogels: From 1D Nanomaterials to 3D Electrically Conductive and Mechanically Resistant Lightweight Architectures

Maribel Touron, Caroline Celle,* Laurent Orgéas, and Jean-Pierre Simonato*

Cite This: https://doi.org/10.1021/acsnano.2c04288

Read Online

ACCESS | Metrics & More | Article Recommendations | Supporting Information

ABSTRACT: The directed assembly of nanomaterials into 3D architectures is a powerful tool to produce macroscopic materials with tailored physical properties. We show in this article that such a process can be advantageously performed for the fabrication of lightweight electrically conductive materials. Silver nanowire aerogels (AgNWAs) with very low densities (down to ~6 mg cm^{-3}) were ice-templated and freeze-dried, leading to 3D shaped cellular materials based on one-dimensional nanoscopic building blocks. Due to their intrinsic moderate mechanical resistance, the potential use of pure AgNWAs in real life applications appears rather limited. We demonstrate that the addition of carboxymethylcellulose (CMC) in a 1:1 weight ratio leads to the fabrication of hybrid aerogels with highly improved mechanical properties. The molecular weight of the CMC is shown to be a critical parameter to ensure a good dispersion of the AgNWs, and thus to reach excellent performances such as a very low resistivity (0.9 ± 0.2 Ω·cm at 99.2 vol % porosity). The combination of silver nanowires with CMC-700k results in a gain higher than 7100% of the Young's modulus, from 10.4 ± 0.9 kPa (at very low density, i.e., 12 mg cm^{-3}) for the AgNWAs to 740 ± 40 kPa for the AgNW:CMC aerogel. Electromechanical characterizations allowed us to quantify the piezoelectric properties of these hybrid aerogels. The very good elasticity and the piezoelectric behavior stability up to 100 cycles of compression under high (50%) deformation were revealed, which may be of interest for various applications such as pressure sensors.
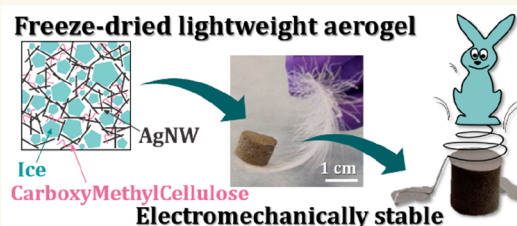
KEYWORDS: *aerogel, freeze-drying, ice-templating, nanowires, cellulose, pressure sensor, piezoresistivity*

Freeze-dried lightweight aerogel. AgNW. Ice. CarboxyMethylCellulose. 1 cm. Electromechanically stable

INTRODUCTION

Highly porous materials such as aerogels, cryogels and foams are currently actively investigated since they combine multiple advantageous properties such as lightweight, high specific surface and low raw material consumption. Thanks to the performances achieved so far, these structures have found a wide range of promising applications such as insulation, depollution, medicine, sensors, to name but a few.[1−7] Among that range of lightweight materials, those made of electrically conductive materials such as metals appear of particular interest. Notwithstanding a highly porous structure, usually higher than 98 vol %, lightweight materials with high electrically conductivity can be obtained. They have already proven efficient in applications such as electronics, catalysis, energy storage and electrochemistry.[8−13]

Although top-down processing routes were mostly preferred until recently, for instance by foaming molten metals by gas injection or investment casting,[11] the development of metallic

nanowires (MNWs) has led to a promising alternative bottom-up route. Mostly copper and silver nanowires-based lightweight structures have been realized up to now. This can be ascribed to their rather straightforward and well developed chemical syntheses.[14−22] Conveniently, Ag and Cu are the two most electrically conductive metals. Based on the use of MNWs, the two most studied routes rely on the fabrication of aerogels through freeze-drying[23−28] or CO$_2$ supercritical drying.[29−31]

This study was carried out with silver nanowires (AgNWs) because silver is the most conductive metal and AgNWs are
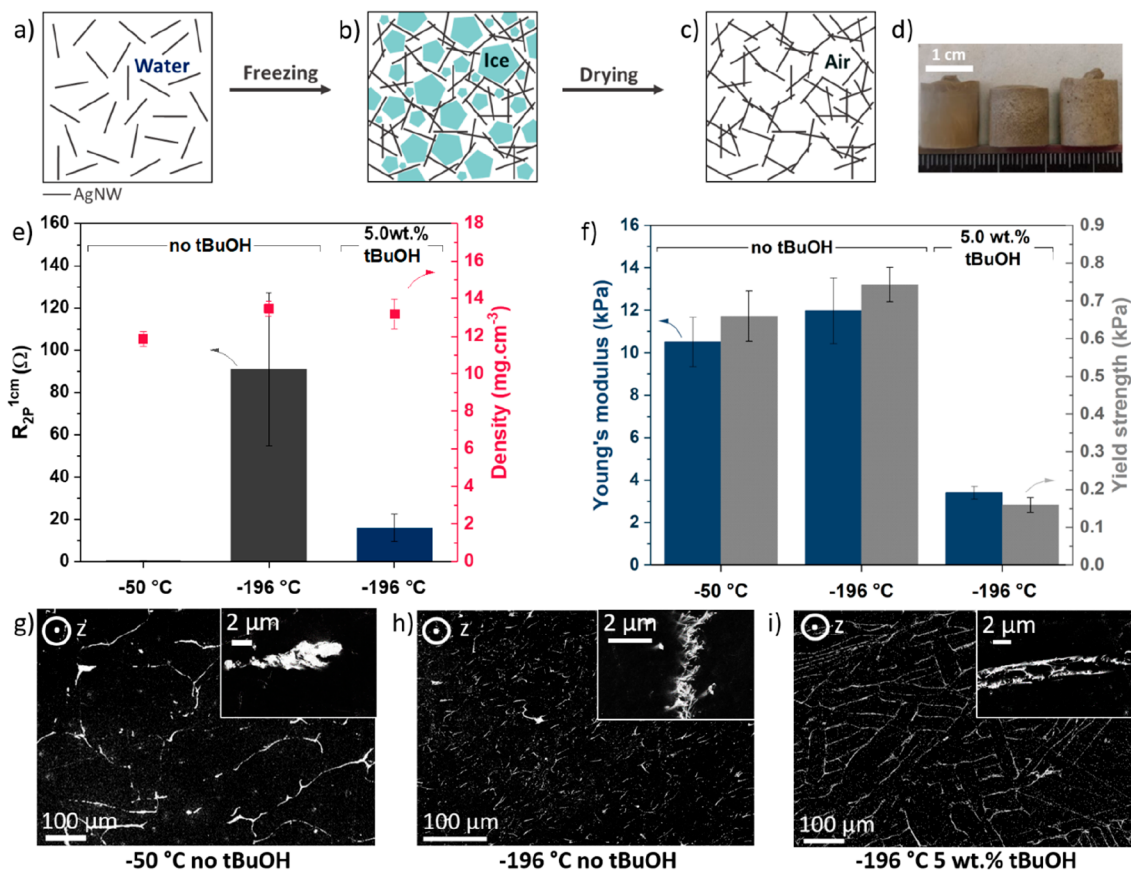
Figure 1. Synthesis of AgNW-based aerogels: Electrical, mechanical and morphological characterizations of pure AgNWAs at 1.0 wt %. (a−c) Schematic representation of the AgNWA synthesis protocol with (a) dispersion of AgNW in liquid water; (b) generation of 3D percolating network of AgNWs during ice-templating and (c) ice sublimation leading to the dried 3D AgNW network. (d) Photograph of three AgNWAs, from left to right frozen at −196 °C without tBuOH, frozen at −50 °C without tBuOH and frozen at −196 °C with 5.0 wt % tBuOH. (e) Electrical resistances and densities of the three AgNWAs. (f) Mechanical properties (Young's modulus and yield strength) of the three aerogels. (g−i) SEM images of AgNWA networks.

less prone to oxidation compared to CuNWs, though the latter could possibly be stabilized by a core−shell structure.[32,33] Also, the AgNWs synthesis is now well-known and mastered.[34−37]

The highly porous structures made of MNWs are very exciting materials and could address various uses. Unfortunately, they demonstrate limited mechanical resistance, which hampers their use for further exploitation.[23] Two main two-step procedures based on hybridation with polymers have been developed to thwart this flaw. The most common one is a process, which consists of dip-coating an insulating lightweight structure in a solution containing MNWs in suspension. After deposition of the MNWs onto the structure, superficial conformal electrically conductive 3D networks can be achieved.[21,38−41] The second route is based on impregnation, typically with polydimethylsiloxane (PDMS), of a pre-existing metallic porous material to ensure mechanical resistance. However, most of the porosity is lost in this case.[25,42,43]

So far, most hybrid structures have been developed with cellulose derivatives polymers,[44,45] polyurethane[46−48] or poly-(vinyl alcohol).[49] Some cellulose-based polymers have already been identified as very efficient stabilizer in 2D networks of MNWs, notably because they facilitate the deposition process and restrain resistive contacts during the fabrication of the random networks, resulting in highly conductive transparent and flexible coatings.[50]

In this article, we demonstrate the interest of ice-templated hybrid cellular materials using both AgNWs and cellulose derivatives. We show that though the synthesis of aerogels made of pure AgNWs with high electrical conductivity is possible, their mechanical properties remain quite limited. However, once hybridated with some specific polymers such as carboxymethylcellulose (CMC), we show that AgNWs give access to mechanically resistant and still highly conductive aerogels. The choice of the polymer is of utmost importance to ensure an optimized 3D percolative network of the metallic nanowires, and thus to maintain a high conductivity throughout the 3D architecture. The piezoresistive behavior of the aerogels was characterized by mechanical cycling tests, and revealed an excellent stability under one hundred cycles at high compression.

RESULTS AND DISCUSSION

Silver Nanowire Aerogels (AgNWAs). We first investigated the microstructure as well as the electrical and mechanical properties of AgNWAs without CMC. More precisely, the role of the freezing temperature as well as the presence of a cryoprotectant on the microstructural and physical properties of AgNWAs was analyzed.[4,29,51,52] We also investigated the effect of AgNW concentration. Thus, several cylindrical samples were produced according to the protocol shown in Figure 1a−c. Because the addition of a
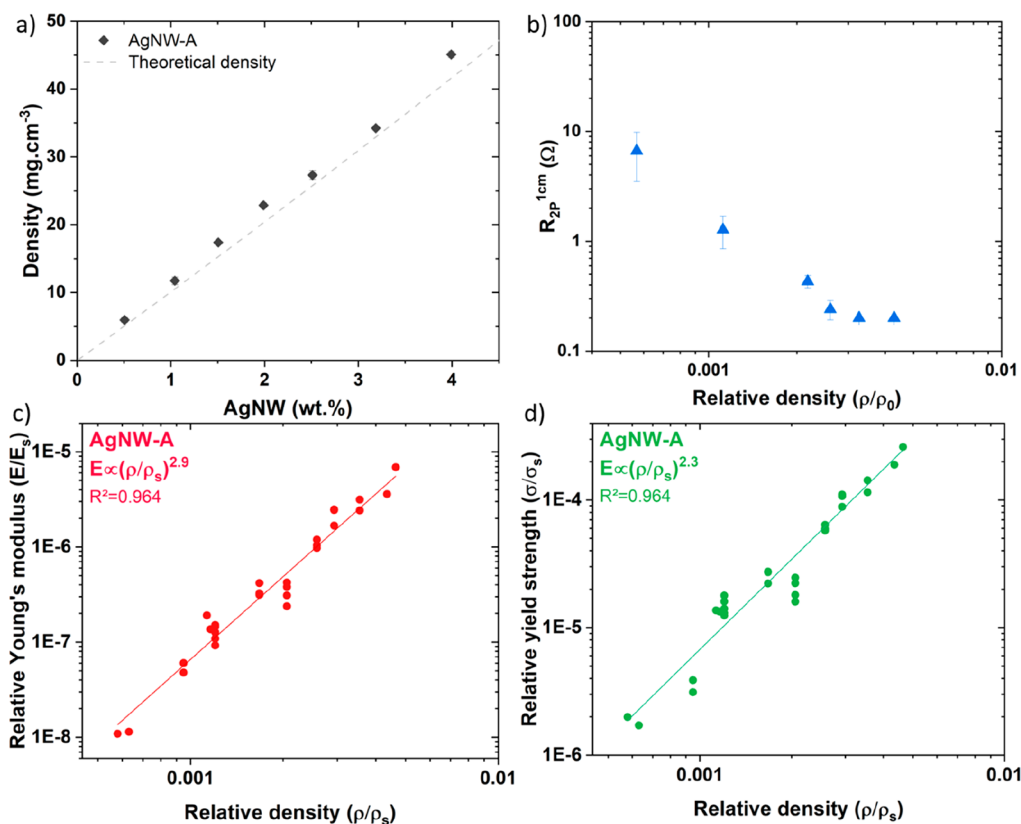
Figure 2. Electrical and mechanical characterizations of pure AgNWA (freeze-dried at −50 °C). (a) Measured and predicted density of the AgNWAs as functions of the AgNW concentration in solution. (b) Evolution of the electrical resistance R_{2P}^{1cm} of AgNWAs with the AgNWA relative density. (c) Relative Young's modulus (E/E_s) as a function of the relative density. (d) Relative yield strength (σ/σ_s) as a function of the relative density. The dotted lines in panels c and d correspond to power laws used to fit experimental data (the corresponding coefficients are displayed on the top left parts of the figures).

cryoprotectant (a substance mainly used in biology and food industry that prevents the tissue deterioration due to ice expansion during freezing) has been advantageously reported, we assessed the potential interest in our synthetic protocol. We used *tert*-butanol (tBuOH) as it (i) sublimates easily with water during the freeze-drying process and (ii) has already proven efficient in some aerogel syntheses.[53] During the freeze-drying process, the water crystallizes and the AgNWs are segregated around the ice crystals.[54] Once located at the boundaries of the ice crystals, the AgNWs form a 3D network that remains practically unchanged after ice sublimation. The aerogel shape can be defined according to the mold geometry, for instance in a cylindrical vessel as shown in Figure 1d.

Effects of Freezing Conditions. First, AgNW solutions at 1.0 wt % in water only were subjected to two freezing temperatures: −50 °C on the freeze-dryer's tray (conditions detailed in Figure S1), which induced a quasi-vertical freezing (along the *z*-direction, which corresponds to the axis of the cylindrical samples), and −196 °C by immersion of the molds into liquid nitrogen. In the second case, a radial directed freezing was observed. Those two protocols resulted into slow and fast freezing rates, respectively. The final densities of 1.0 wt % AgNWA were measured at 13.0 ± 1.0 mg cm$^{−3}$, whatever the freezing mode (Figure 1e). This density is consistent with the one estimated theoretically from the AgNW weight content. In addition, the whole processed samples exhibited nice cylindrical shape. These two observations indicate a negligible and homogeneous shrinkage during the freeze-drying process. Moreover, as shown in Figure 1g, at a given

volume and identical compositions, the microstructure of AgNWs within the aerogels are driven by the process parameters. When the samples are slowly frozen, the growth of ice crystals is favored, which results in aerogels exhibiting large pores (242 ± 50 μm perpendicular to the *z*-axis) as shown in Figure 1g. When the applied freezing rate is faster, the crystal seed density is increased and ice-crystal growth is restrained. The pores are not so well-defined and their average diameter drops down to 5 ± 2 μm (Figure 1h.). These changes of microstructures alter the macroscale electrical and mechanical properties. For instance, for the AgNWA fabricated at −50 °C the electrical resistance at 1 cm (R_{2P}^{1cm}) was 0.5 Ω, whereas it rose up to 86 Ω for the AgNWA prepared at −196 °C, as displayed in Figure 1e: as the cell-wall density in AgNWa freezed at −50 °C is higher, more electrical pathways are formed, which induces a decrease of the electrical resistance. Also, it is worth noting that no significant impact of the freezing rate on the mechanical stiffness and resistance was observed: the Young's moduli and yield strengths of AgNWAs prepared at −50 and −196 °C were measured at 10.4 ± 0.9 kPa, 0.62 ± 0.04 kPa and 12.0 ± 1.5 kPa, 0.74 ± 0.05 kPa, respectively (Figure 1.f.).

Effects of Cryoprotectant. Mixtures of water and tBuOH resulted in aerogels with smaller pores and yielded smaller crystal sizes depending on the freezing conditions.[55] Only the data obtained with the aerogels frozen at −196 °C are presented herein because the samples with tBuOH frozen at −50 °C could not be unmolded properly due to mechanical instability, leading to the collapse of the structure. The
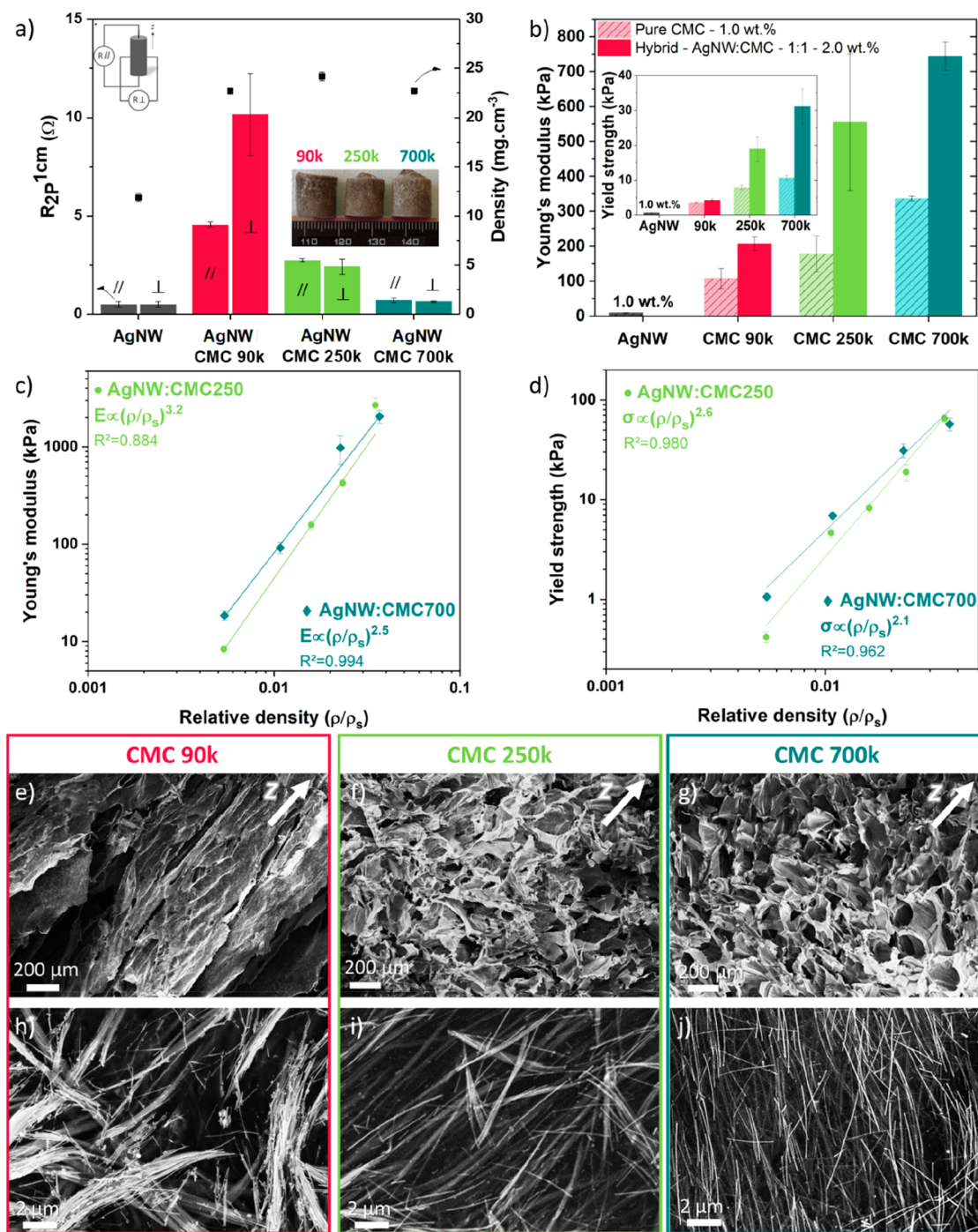
Figure 3. Electrical, mechanical and morphological characterizations of AgNW:CMC aerogels with three different cellulosic polymers. Selected molecular weights of CMC are 90k (red), 250k (green) and 700k (blue). Freezing conditions set at −50 °C. AgNW:CMC ratios are set to 1:1 in weight. (a) R_{2P}^{1cm} (left) and density (right) of AgNWA (in dark gray) and AgNW:CMC aerogels with CMC molecular weight of 90k, 250k and 700k; schematic view of perpendicular and parallel electrical measurements (left upper corner) and optical pictures of AgNW:CMC aerogels (inset). (b) Young's modulus of pure CMC (dashed bars) and hybrid (plain bars) aerogels. (c) Young's modulus and (d) yield strength of hybrid aerogels with CMC 250k and 700k, as a function of their relative densities and corresponding fitted power-laws. (e−j) SEM images of AgNW:CMC aerogels with different magnifications for CMC molecular weight of (e and h) 90k, (f and i) 250k, and (g and j) 700k. White arrows represent the z-axis of the structure parallel to the freeze-drying front.

resulting microstructures are very different from those obtained without tBuOH. For example, the cross section displayed in Figure 1I shows a lamellar structure of this material with pores of 133 ± 34 μm average length and 33 ± 7 μm average width. Such lamellae were not observed without tBuOH, and the pores appear significantly larger. This

structural modification resulted in important changes on both electrical and mechanical properties of the aerogel. Thus, R_{2P}^{1cm} was measured at 18 Ω, i.e., 65% lower than samples without tBuOH. Similarly to AgNWA fabricated at −50 °C, AgNWA-tBuOH had bigger pores and thicker and presumably denser pore walls, resulting in a higher number of electrical

contacts between AgNWs, and therefore a lower electrical resistance. More importantly, both Young's modulus and yield strength were, however, divided by 4 compared to free-tBuOH samples (3.4 ± 0.3 kPa and 0.16 ± 0.02 kPa against 12.0 ± 1.5 kPa, 0.74 ± 0.05 kPa for AgNWA-tBuOH-196 °C and AgNWA-196 °C respectively), which could be detrimental for some applications. Since AgNWA fabricated at −50 °C displayed the best electrical and mechanical properties, the study was then carried out by freezing on the trays at −50 °C, without addition of tBuOH.

Effects of AgNW Concentration. We first assessed the impact of the AgNW initial concentration on the density of the aerogels. We found that the measured density of the aerogels increases linearly as a function of the AgNW concentration in the solution, as shown in Figure 2a. The theoretical density (dotted line in the figure) was calculated from the initial volume of the solution and the corresponding weight of AgNWs. The AgNWA experimental densities are close to the theoretical density, indicating once again that the shrinkage due to the freeze-drying is very limited, in the range from 0.5 to 4.0 wt %. Concurrently, when the AgNW loading is increased from 0.5 to 4.0 wt %, the electrical resistance R_{2P}^{1cm} decreases from 6.7 to 0.2 Ω (Figure 2b), which is probably due to an increase of electrical contacts throughout the volume with the concentration of AgNWs.[56]

In addition, the compression stress−strain curves of AgNWAs with different AgNW concentrations are shown in Figure S2. Stress−strain curves are very different from those observed during the compaction of elastic homogeneous entangled fibrous materials.[57−61] They rather resemble to those observed in numerous elasto-plastic cellular materials with (or without) cell walls,[62,63] i.e., with first a linear region (apparently elastic) up to a yield strength that is followed by a marked elastoplastic stress plateau characterizing an easy densification phase, followed by a more difficult densification phase with a sharp increase of stress levels. The AgNWA elastoplastic plateau reaches a compression strain up to 0.6 when the AgNW concentration ranges from 0.5 to 3.0 wt % and up to 0.5 at 4.0 wt %. As for other cellular materials, the mechanical stiffness and resistance of AgNWAs strongly depend on their relative density[62] and thus on the AgNW concentration. Hence, from 0.5 wt % (for a density of 6.1 ± 0.3 mg.cm^{-3}) to 4.0 wt % of AgNW loading (density of 45.1 ± 2.0 mg.cm^{-3}), the Young's modulus was increased from 0.8 to 480 kPa. To the best of our knowledge, this is the highest Young's modulus reported so far for pure metallic nanowire aerogels. More precisely, Figure 2.c-d. shows the evolution of the relative Young's modulus and yield strength as a function of the relative density ρ/ρ_s of the AgNWAs, ρ and ρ_s being the density of the AgNWAs and AgNWs, respectively. Both of them rapidly increase with the relative density and follow power-laws, as often observed for cellular materials.[62] Here, the power-law exponents are $n = 2.9 \pm 0.1$ and $m = 2.3 \pm 0.1$ for the Young's modulus and the yield strength, respectively. These exponents are in-line with those already observed for other stochastic foams made of CuNWs or CNTs.[24,51−53] The value of n is also consistent with that found by Qian et al.[23] for similar AgNWAs, i.e., $n = 2.4$ for the relative Young's modulus as a function of the relative density for AgNWAs, and the scaling exponent of 3 reported by Tang et al. for CuNWs aerogels.[24]

Silver Nanowires−CMC Hybrid Aerogels. It is worth noticing that, even with an AgNW concentration of 4.0 wt %

and a density of 45.1 mg cm^{-3}, AgNWAs respectively exhibit a Young's modulus and a yield strength of 480 and 11 kPa only. Though these are high values for such materials, they remain rather moderate at low AgNW concentrations, which could be detrimental for some applications. They are mainly ascribed to the very high porosity of the aerogel (99.6%) but also to the weak and presumably poorly cohesive nanowire−nanowire interactions. Therefore, we added CMC to the AgNW aqueous solution in order to assess its effects on the reinforcement of the resulting freeze-dried aerogels and thus to overcome the aforementioned problem. We chose CMC among a wide variety of polymers because of its good ability to disperse AgNW and its low impact on the electrical conductivity of percolative 2D networks. In addition, CMC is easily processed in water, which is convenient for freeze-drying. The polymer can constitute a self-supporting material even if the AgNWs do not percolate within the CMC matrix. Electrical, mechanical and morphological properties of these hybrid aerogels are reported in Figure 3.

With the addition of CMC, the total weight loading is doubled from 1.0 wt % of AgNW to 2.0 wt % of AgNW and CMC. The densities of the hybrid aerogels almost double from 12.0 ± 1 mg·cm^{-3} to 23.2 ± 0.7 mg·cm^{-3}, indicating that the shrinkage due to the freeze-drying process is also very limited for the hybrid aerogels.

Even with the polymer addition, the values of R_{2P}^{1cm} remain low, all of them being lower than 10 Ω for the three CMCs with various molecular weights (Figure 3a). It is observed that the R_{2P}^{1cm} decreases when the molecular weight of the CMC increases. This is attributed to a better dispersion of the AgNWs in the CMC 700k than in the CMC 250k and even more than in the CMC 90k, as clearly observable on the scanning electron microscopy (SEM) images focused on the pore walls of the aerogels (Figure 3h−j). The viscosities of CMC dispersions increase with the CMC's molecular weight (Table S1), certainly due to enhanced entanglement of longer polymer chains. The viscosity in the CMC 700k dispersion appears sufficient to block the formation of AgNWs bundles during the freeze-drying process, which leads to the presence of more dispersed nanowires within the matrix. This results in an extended 3D connectivity of the nanowire network, and *in fine* in a lower electrical resistance of the aerogel as shown in Figure 3a.

Another significant effect that depends on the CMC molecular weight is the lamellar structuration of the AgNW:CMC 90k aerogel (Figure 3e). The ice crystal growth is favored in a less viscous solution: ice lamellae can grow along the freezing axis. Consequently, anisotropic lamellae of AgNW and CMC pore walls are formed and thus the R_{2P}^{1cm} of this aerogel is spatially different with a lower resistance (4.6 ± 0.2 Ω at 1 cm) along the freezing axis compared to the perpendicular axis (10.2 ± 2.1 Ω at 1 cm). On the contrary, both AgNW:CMC 250k and 700k aerogels resulting from more viscous solutions exhibit more isotropic cellular structures (Figure 3f,g) and therefore isotropic values of R_{2P}^{1cm}. A SEM image of a pure CMC 700k aerogel is shown if Figure S3 for comparison. As already observed for AgNWA without CMC, when the porosity decreases (i.e., when the total concentration increases), the electrical conductivity of the samples increases because more electrical pathways are created. The electrical resistance and resistivity of hybrid aerogels made of AgNW and CMC 700k at different weight ratios and total concentrations are presented in Table S2.
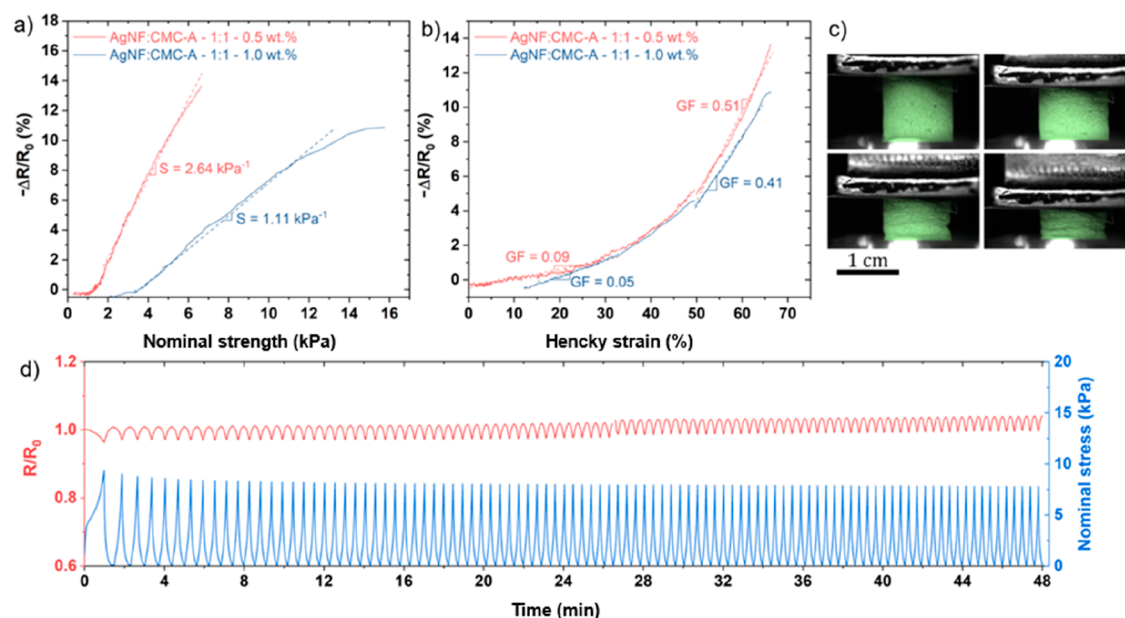
Figure 4. Electromechanical characterizations of AgNW:CMC hybrid aerogels. Freezing conditions were set at −50 °C. (a) Sensitivity and (b) gauge factor for AgNW:CMC 700-1:1-0.5 wt % and AgNW:CMC700-1:1-1.0 wt % aerogels. (c) Photographs of AgNW:CMC 700k ratio of 1:1 and 1.0 wt % at 4 different stages of compression. (d) Mechanical stability over a hundred cycles at the same maximum compressive displacement of half of the sample height. The composition of the sample is AgNW:CMC 700k ratio of 1:1 in weight and total concentration of 1.0 wt %.

The Young's moduli and the yield strengths of aerogels with a single component, either AgNW or CMC, or hybrid aerogels are shown in Figure 3b. Adding 1.0 wt % of CMC to 1.0 wt % of AgNWs resulted in a dramatic increase in Young's modulus and yield strength for the three CMCs. For instance, the comparison of a pure AgNWA with the AgNW:CMC-700k hybrid aerogel shows a Young's modulus gain higher than 7100% from 10.4 to 740 kPa and a 50-fold yield strength increase from 0.62 to 31 kPa. Such an increase was unexpected and resulted from a great synergetic effect. Indeed, the neat CMC-based aerogels present significantly lower Young's modulus and yield strength. For instance, the comparison of pure CMC-based aerogels properties compared to AgNW:CMC-700k aerogels results in a large Young's modulus improvement from 336 to 740 kPa and a nearly 3-fold yield strength gain from 10.6 to 31.1 kPa. The neat CMC 700k-based aerogel displays the higher mechanical resistance of the three CMCs, and logically the hybrid aerogel AgNW:CMC 700k exhibits the highest mechanical resistance.

The evolution of the Young's modulus and the yield strength with the relative density of two hybrid aerogels (weight ratio of AgNW/CMC = 1) is presented in Figure 3c,d. For AgNW:CMC 250k, the scaling exponents of $n = 3.2 \pm 0.1$ for the Young's modulus and $m = 2.6 \pm 0.1$ for the yield strength are consistent with other stochastic foams for which parameters are $3 < n < 4$ and $2.5 < m < 3.5$. The Young's modulus of AgNW:CMC 700k appears to scale of with $(\rho/\rho_s)^{2.5}$. Concerning AgNW:CMC 700k, the scaling exponents of $n = 2.5 \pm 0.1$ for the Young's modulus and $m = 2.1 \pm 0.1$ for the yield strength are closer to the scaling exponents of open cells porous materials than to stochastic foams.

Electromechanical Characterizations. We then investigated the capability of the AgNW:CMC aerogels to be used as lightweight pressure sensors. To this end, we developed a test bench to measure simultaneously electrical and mechanical properties (Figure S4). The compression cycles did not induce

any significant degradation of the electrical conductivity after 5 cycles with a maximal deformation of 2/3 of the height of the sample (Figure S5). Therefore, the AgNW percolating network within the CMC is not significantly degraded, the pore walls were mainly elastically deformed and not broken by the compression cycles. This demonstrates that the CMC affords an efficient elasticity to the composite aerogels at 0.5 wt % and at 1.0 wt %.

When the total concentration is divided by 2 from 1.0 to 0.5 wt % at the same weight ratio of 1:1, the nominal applied stress for the same maximal displacement is lowered by 57% (from 16.5 down to 7.0 kPa). The aerogel becomes less mechanically resistant and the force needed to reach the same relative deformation of 2/3 of the height of the sample is significantly lowered. This points out that the mechanical resistance of the aerogels is largely tunable with the total concentration used at the synthesis stage.

Both AgNW:CMC 700-1:1-0.5 wt % and AgNW:CMC700-1:1-1.0 wt % aerogels were compared for their stress sensitivity (S) and their strain gauge factor (GF) during compression up to a 70% compression strain. Corresponding stress−strain and resistivity−strain curves are reported in Figure S6, and an example of the sample compression-induced deformation is shown in Figure 4c. Those two figures prove that the produced aerogels exhibit a typical elastoplastic compression behavior with (i) a first sharp increase of stress levels (apparent elastic regime) (ii) followed by a softer compression plateau with weak strain hardening of stress levels during which consolidation occurs without marked Poisson effects, (iii) noticeable elastic recovery even at high compression strains, such a recovery being more efficient to that observed for AgNW aerogels (Figure S2), (iv) stress levels two to three times higher for 1 wt % aerogel, (v) noticeable strain-induced decrease of the foam resistivity. The corresponding stress sensitivities S and strain gauge factors GF are displayed in Figure 4a,b. It is interesting to notice that after the apparent

elastic domain (for strains below 10% where S is practically zero-valued), S becomes finite and constant. The sensitivity for the 0.5 wt % aerogel is measured at 2.64 k·Pa^{-1}, which compares very well with the state of the art of similar lightweight materials.[45,64−66] It is also worth noting that S diminishes with the solid content. This is ascribed to a strain hardening of stress levels that is more pronounced for the 1 wt % aerogels (see Figure S6). In addition, Figure 4b shows that the strain gauge factor GF is not constant but evolves as a power-law function of the compression strain (and thus of the solid content), whatever the considered aerogels: increasing the compression strain leads to increase the solid content, which in turn increases the AgNW connectivity, and thus GF.

Figure 4d shows the stability study of a AgNW:CMC700-1:1-1.0 wt % aerogel enduring a hundred compressions at the same maximum displacement (half of its initial height, i.e., at a 70% compression strain, 100 cycles in 48 min). After the first compression, the R/R_0 variation from zero pressure to the maximum stress is measured at −4.5%. After 100 cycles, the R/R_0 variation is very similar at −4.2%. In addition, the R/R_0 value without applied pressure between the first and the 100th cycles raised only from 1.02 to 1.04. In a complementary measurement, the value of R/R_0 under the maximal stress between the first and the 100th cycles increased slightly from 0.97 to 0.99. Therefore, the degradation of the electromechanical properties of the aerogel appears very limited after 100 compressions at a severe compression strain.

The composition of the aerogels can be adjusted on demand. For instance adding polymer allows to drastically improve the mechanical resistance of the sample, and reducing the weight ratio of AgNW/CMC leads to an increase of the R/R_0 variation range. Hence, by modifying the composition of the aerogel it is possible to fine-tune the sensor sensitivity.

CONCLUSIONS

In summary, extremely lightweight metallic materials (down to 6 mg cm^{-3}) were synthesized by ice templating one-dimensional silver nanostructures and freeze-drying. These aerogels exhibit very good electrical conduction properties, but their intrinsic mechanical resistance is somewhat limited. The fabrication of hybrid aerogels relying on the addition of CMC results in a dramatic improvement of the mechanical resistance (above 7000%), while keeping excellent electrical conductivity (0.9 ± 0.2 Ω·cm at 1:1 AgNW/CMC ratio, and 2.0 wt % total). The molecular weight of the CMC was shown to play a crucial role to enhance the 3D percolative network through higher dispersion of the AgNWs with the CMC matrix and thus to strengthen both the mechanical and electrical properties of ice-templated aerogels. Moreover, the values of the Young's modulus are among the highest reported so far for very lightweight aerogels (<25 mg cm^{-3}). Finally, electromechanical characterization revealed that hybrid aerogels with AgNWs and CMC are piezoresistive with a very stable electromechanical behavior over a hundred cycles performed at severe compression strains. We think that the reported approach could expand the materials portfolio of lightweight electrically conductive materials, which are of interest for a wide set of applications including pressure sensors.

MATERIALS AND METHODS

Chemical Reagents. Carboxymethylcellulose (CMC) with molecular weights of 90, 250 and 700 kg mol^{-1} and tBuOH were purchased from Sigma-Aldrich and used without further purification.

Synthesis and Purification of AgNWs. In a typical synthesis, AgNO$_3$ (0.68 g) was dissolved in EG (40 mL) at a slow stirring rate in a round flask. In another flask, polyvinylpyrrolidone (PVP, average mol. wt. 40 000, 1.77 g), NaCl, was dissolved in EG (80 mL) at 120 °C. The solution was cooled to room temperature and then slowly added to the first flask within 8 min. The mixture was finally heated at 160 °C and cooled down at ambient temperature. To remove EG and PVP, the purification of the AgNWs was first realized by decantation. The settled product that contains the AgNWs was redispersed into a minimal amount of water. Then three consecutives steps with acetone flocculation and water washing were carried out. After this purification process, only a thin layer of PVP remained around the AgNWs.[35,38,67] Resulting AgNWs exhibited a mean diameter of 55 ± 13 nm and an average length of 6.8 ± 3.8 μm.

Synthesis of AgNW Aerogels (AgNWA). AgNWs were dispersed at the desired concentration (wt %) in water under gentle mechanical agitation. tBuOH was then added to the dispersion at a concentration of 5.0 wt % for samples named AgNWA-tBuOH. Then, 1.5 g of this solution was poured into a flat bottom cylindrical flask with straight edge. The molds were then inserted into a MUT 004 A benchtop pilot freeze-dryer from Cryotec with cooling trays. The temperature evolution of the trays as well as the pressure in the chamber are reported in Figure S1. Freezing by immersion of the molds into liquid N$_2$ was also performed for the samples called AgNWA-liqN2, i,e, without tBuOH. After freezing, the lyophilization was performed as explained before, but starting directly from the plateau at −50 °C and atmospheric pressure.

Synthesis of Hybrid AgNW:CMC Aerogels (AgNW:CMC-A). The CMC was added into water and dispersed at 60 °C under vigorous agitation. AgNWs were dispersed in water. Both solutions were mixed together at 120 rpm at room temperature. The sum of both polymer and AgNWs concentrations at this step is named total load in wt %. The solutions were left 21 h at room temperature in hermetically closed vials without agitation. Then, the solutions were agitated at 120 rpm at room temperature for 3 h and 1.5 g of this solution was poured into a cylindrical flask. The molds were then inserted into the MUT 004 A benchtop pilot freeze-dryer from Cryotec. Then, the protocol of freeze-drying was identical to AgNWA.

Two-Probes Electrical Resistance at 1 cm (R_{2P}^{1cm}). An IDM19 pocket multimeter from RS components was used to measure the electrical resistance. The probes were separated by 1 cm. Small droplets of GaIn eutectic were used to ensure good electrical contacts between the probes and the aerogels.

SEM Analysis. Electrically conductive samples were cut longitudinally and transversally and their micro and nanostructures were observed in a SEM Zeiss Ultra. For that purpose, a 10 nm layer of Pt was deposited with a Biorad sputter coater SC500 on nonelectrically conductive aerogels made of neat CMC prior to SEM observation. In addition, AgNWA were impregnated with an epoxy resin and polished before SEM characterization.

Compressive Mechanical Resistance. To characterize the mechanical properties of the AgNW-based aerogels, uniaxial compression tests were performed on cylindrical samples (initial diameter $d_0 \approx 11$ mm and initial height $h_0 \approx 10$ mm) using an electromechanical testing machine (Instron 5960, USA) equipped with a force sensor of 10 N or 5 kN and compression platens. During the tests, the actual sample height h together with the compression forces F were recorded so that the nominal compression stress $\sigma_0 = 4|F|/(\pi d_0^2)$ and the Hencky strain $\varepsilon = |\ln(h/h_0)|$ could be estimated to build stress−strain curves. Tests were achieved at a constant compression velocity $|\dot{h}|$ with an initial strain rate $|\dot{\varepsilon}_0| = |\dot{h}|/h_0 = 0.01$ s^{-1}. As shown in the typical stress−strain curve $\sigma_0(\varepsilon)$ of Figure S2, a first compression loading was carried out up to a small strain $|\varepsilon| = 5\%$, then sample were unloaded. The early stage of this unloading phase was used to estimate the sample Young moduli. Therefrom, the sample were reloaded up to $|\varepsilon| = 70\%$ and unloaded again. From this sequence, the compression yield strength was also assessed, as sketched in Figure S2.

Electromechanical Measurements. To assess the evolution of the sample conductivity upon mechanical cycling, we performed in

situ conductivity measurement during cyclic compression tests. For that purpose, electrically conductive silver paint (Conductive Silver Lacquer L200N from Ferro) was used to glue the aerogel samples on a PEN (polyethylene naphthalate) substrate. An electric track was also drawn from the sample to one border of the substrate. The upper face of the aerogel sample was stuck onto a thinner PEN foil with silver paint. Three 25 μm diameter Au wires from Heraeus were used to make the electrical junctions between the upper face of the aerogel and a second silver paint electric track on the substrate. The electric grippers connected to a Keysight B2902A potential and current alimentation were pinched on metallic adhesives connected to both silver paint tracks. Constant potential was applied during the compression cycles and both potential and current were measured every 0.01 s with a holding time of 0.02 s. The noise from the measured signals was removed with Origin Lab' signal processing filtering method of Savitzky-Golay on a window size of 100 points. The compression cycles that were carried out during electrical measurements consisted in a first loading up to $|\varepsilon| = 5\%$, followed by unload and reload sequences up to $|\varepsilon| = 27.5\%$, 55%, 82.5% and 110%, respectively. Then, last, samples were subjected to 100 cycles of unload–reload at this maximal compression strain.

ASSOCIATED CONTENT

ⓢ Supporting Information

The Supporting Information is available free of charge at https://pubs.acs.org/doi/10.1021/acsnano.2c04288.

> Program of temperature and pressure of the freeze-drying process (Figure S1); compressive stress–strain curves $\sigma_0(\varepsilon)$ of AgNWA (Figure S2); instantaneous shear viscosity of water dissolutions of CMCs with three different molecular weights (Table S1); electrical resistance and resistivity of hybrid aerogels made of AgNW and CMC 700k at different weight ratios and total concentrations (Table S2); SEM micrograph of a pure CMC 700k aerogel (FigureS3); set-up for characterizing the electromechanical properties (Figure S4); electromechanical characterization of AgNW:CMC hybrid aerogels for five incremental compressions, effect electrical resistance and nominal stress (Figure S5); compressive stress–strain curves $\sigma_0(\varepsilon)$ and resistance variation of AgNWA (Figure S6)(PDF)

AUTHOR INFORMATION

Corresponding Authors

Caroline Celle — *University Grenoble Alpes, Grenoble 38000, France*; Email: caroline.celle@cea.fr

Jean-Pierre Simonato — *University Grenoble Alpes, Grenoble 38000, France*; ⓞ orcid.org/0000-0002-0217-4237; Email: jean-pierre.simonato@cea.fr

Authors

Maribel Touron — *University Grenoble Alpes, Grenoble 38000, France*

Laurent Orgéas — *University Grenoble Alpes, Grenoble 38000, France*; ⓞ orcid.org/0000-0003-1668-688X

Complete contact information is available at:
https://pubs.acs.org/10.1021/acsnano.2c04288

Notes

The authors declare no competing financial interest.

REFERENCES

(1) Fischer, F.; Rigacci, A.; Pirard, R.; Berthon-Fabry, S.; Achard, P. Cellulose-Based Aerogels. *Polymer* **2006**, *47* (22), 7636–7645.

(2) Bryning, M. B.; Milkie, D. E.; Islam, M. F.; Hough, L. A.; Kikkawa, J. M.; Yodh, A. G. Carbon Nanotube Aerogels. *Adv. Mater.* **2007**, *19* (5), 661–664.

(3) Gorgolis, G.; Galiotis, C. Graphene Aerogels: A Review. *2D Mater.* **2017**, *4* (3), 032001.

(4) Ahankari, S.; Paliwal, P.; Subhedar, A.; Kargarzadeh, H. Recent Developments in Nanocellulose-Based Aerogels in Thermal Applications: A Review. *ACS Nano* **2021**, *15*, 3849.

(5) Mazrouei-Sebdani, Z.; Begum, H.; Schoenwald, S.; Horoshenkov, K. V.; Malfait, W. J. A Review on Silica Aerogel-Based Materials for Acoustic Applications. *J. Non-Cryst. Solids* **2021**, *562*, 120770.

(6) Zhang, X.; Zhou, J.; Zheng, Y.; Wei, H.; Su, Z. Graphene-Based Hybrid Aerogels for Energy and Environmental Applications. *Chem. Eng. J.* **2021**, *420*, 129700.

(7) Chen, Y.; Zhang, L.; Yang, Y.; Pang, B.; Xu, W.; Duan, G.; Jiang, S.; Zhang, K. Recent Progress on Nanocellulose Aerogels: Preparation, Modification, Composite Fabrication, Applications. *Adv. Mater.* **2021**, *33* (11), 2005569.

(8) Zhu, C.; Du, D.; Eychmüller, A.; Lin, Y. Engineering Ordered and Nonordered Porous Noble Metal Nanostructures: Synthesis, Assembly, and Their Applications in Electrochemistry. *Chem. Rev.* **2015**, *115* (16), 8896–8943.

(9) Liu, W.; Herrmann, A.-K.; Bigall, N. C.; Rodriguez, P.; Wen, D.; Oezaslan, M.; Schmidt, T. J.; Gaponik, N.; Eychmüller, A. Noble Metal Aerogels—Synthesis, Characterization, and Application as Electrocatalysts. *Acc. Chem. Res.* **2015**, *48* (2), 154–162.

(10) Kränzlin, N.; Niederberger, M. Controlled Fabrication of Porous Metals from the Nanometer to the Macroscopic Scale. *Mater. Horiz.* **2015**, *2* (4), 359–377.

(11) Banhart, J. Manufacture, Characterisation and Application of Cellular Metals and Metal Foams. *Prog. Mater. Sci.* **2001**, *46* (6), 559–632.

(12) Atwater, M. A.; Guevara, L. N.; Darling, K. A.; Tschopp, M. A. Solid State Porous Metal Production: A Review of the Capabilities, Characteristics, and Challenges. *Adv. Eng. Mater.* **2018**, *20* (7), 1700766.

(13) Yang, F.; Kim, M. J.; Brown, M.; Wiley, B. J. Alkaline Water Electrolysis at 25 A cm^{-2} with a Microfibrous Flow-through Electrode. *Adv. Energy Mater.* **2020**, *10* (25), 2001174.

(14) Bobinger, M.; Dergianlis, V.; Albrecht, A.; Haider, M.; Hirmer, Q.; Becerer, M.; Lugli, P. Solution Processing of Silver Nanowires for Transparent Heaters and Flexible Electronics. *2017 IEEE 13th Conference on Ph.D. Research in Microelectronics and Electronics*, Giardini Naxos, Italy, June 12–15, 2017; IEEE: New York, 2017; pp 9–12. DOI: 10.1109/PRIME.2017.7974094.

(15) Celle, C.; Mayousse, C.; Moreau, E.; Basti, H.; Carella, A.; Simonato, J.-P. Highly Flexible Transparent Film Heaters Based on Random Networks of Silver Nanowires. *Nano Res.* **2012**, *5* (6), 427–433.

(16) Kim, S.; Lee, S. J.; Cho, S.; Shin, S.; Jeong, U.; Myoung, J.-M. Improved Stability of Transparent PEDOT:PSS/Ag Nanowire Hybrid Electrodes by Using Non-Ionic Surfactants. *Chem. Commun.* **2017**, *53* (59), 8292–8295.

(17) Liang, J.; Jiang, C.; Wu, W. Toward Fiber-, Paper-, and Foam-Based Flexible Solid-State Supercapacitors: Electrode Materials and Device Designs. *Nanoscale* **2019**, *11* (15), 7041–7061.

(18) Ma, C.; Gao, X.-M.; Bi, Y.-G.; Zhang, X.-L.; Yin, D.; Wen, X.-M.; Liu, Y.-F.; Feng, J.; Sun, H.-B. PFSA-Passivated Silver Nanowire Transparent Electrodes for Highly Flexible Organic-Light-Emitting Devices with Improved Stability. *Org. Electron.* **2020**, *84*, 105727.

(19) Alshammari, W.; Patil, D. S.; Pawar, S. A.; Shin, J. C. Silver Nanowires-Copper Sulfide Core/Shell Nanostructure for Electrochemical Supercapacitors. *Mater. Today Chem.* **2017**, *5*, 72−80.

(20) Lin, J.-Y.; Huang, J.-J.; Hsueh, Y.-L.; Zhang, Y.-X. Diameter Effect of Silver Nanowire Doped in Activated Carbon as Thin Film Electrode for High Performance Supercapacitor. *Appl. Surf. Sci.* **2019**, *477*, 257−263.

(21) Moon, I. K.; Yoon, S.; Oh, J. 3D Highly Conductive Silver Nanowire@PEDOT:PSS Composite Sponges for Flexible Conductors and Their All-Solid-State Supercapacitor Applications. *Adv. Mater. Interfaces* **2017**, *4* (22), 1700860.

(22) Hanauer, S.; Celle, C.; Crivello, C.; Szambolics, H.; Muñoz-Rojas, D.; Bellet, D.; Simonato, J.-P. Transparent and Mechanically Resistant Silver-Nanowire-Based Low-Emissivity Coatings. *ACS Appl. Mater. Interfaces* **2021**, *13* (18), 21971−21978.

(23) Qian, F.; Lan, P. C.; Freyman, M. C.; Chen, W.; Kou, T.; Olson, T. Y.; Zhu, C.; Worsley, M. A.; Duoss, E. B.; Spadaccini, C. M.; Baumann, T.; Han, T. Y.-J. Ultralight Conductive Silver Nanowire Aerogels. *Nano Lett.* **2017**, *17* (12), 7171−7176.

(24) Tang, Y.; Yeo, K. L.; Chen, Y.; Yap, L. W.; Xiong, W.; Cheng, W. Ultralow-Density Copper Nanowire Aerogel Monoliths with Tunable Mechanical and Electrical Properties. *J. Mater. Chem. A* **2013**, *1* (23), 6723−6726.

(25) Gao, H.-L.; Xu, L.; Long, F.; Pan, Z.; Du, Y.-X.; Lu, Y.; Ge, J.; Yu, S.-H. Macroscopic Free-Standing Hierarchical 3D Architectures Assembled from Silver Nanowires by Ice Templating. *Angew. Chem., Int. Ed.* **2014**, *53* (18), 4561−4566.

(26) Xu, X.; Wang, R.; Nie, P.; Cheng, Y.; Lu, X.; Shi, L.; Sun, J. Copper Nanowire-Based Aerogel with Tunable Pore Structure and Its Application as Flexible Pressure Sensor. *ACS Appl. Mater. Interfaces* **2017**, *9* (16), 14273−14280.

(27) Phattharasupakun, N.; Wutthiprom, J.; Duangdangchote, S.; Sawangphruk, M. A 3D Free-Standing Lithiophilic Silver Nanowire Aerogel for Lithium Metal Batteries without Lithium Dendrites and Volume Expansion: *In Operando* X-Ray Diffraction. *Chem. Commun.* **2019**, *55* (40), 5689−5692.

(28) Zhang, L.; Liu, X.; Deb, A.; Feng, G. Ice-Templating Synthesis of Hierarchical and Anisotropic Silver-Nanowire-Fabric Aerogel and Its Application for Enhancing Thermal Energy Storage Composites. *ACS Sustain. Chem. Eng.* **2019**, *7* (24), 19910−19917.

(29) Fears, T. M.; Hammons, J. A.; Sain, J. D.; Nielsen, M. H.; Braun, T.; Kucheyev, S. O. Ultra-Low-Density Silver Aerogels via Freeze-Substitution. *APL Mater.* **2018**, *6* (9), 091103.

(30) Jung, S. M.; Jung, H. Y.; Dresselhaus, M. S.; Jung, Y. J.; Kong, J. A Facile Route for 3D Aerogels from Nanostructured 1D and 2D Materials. *Sci. Rep.* **2012**, *2* (1). DOI: 10.1038/srep00849.

(31) Jung, S. M.; Preston, D. J.; Jung, H. Y.; Deng, Z.; Wang, E. N.; Kong, J. Porous Cu Nanowire Aerosponges from One-Step Assembly and Their Applications in Heat Dissipation. *Adv. Mater.* **2016**, *28* (7), 1413−1419.

(32) Lee, H.; Hong, S.; Lee, J.; Suh, Y. D.; Kwon, J.; Moon, H.; Kim, H.; Yeo, J.; Ko, S. H. Highly Stretchable and Transparent Supercapacitor by Ag−Au Core−Shell Nanowire Network with High Electrochemical Stability. *ACS Appl. Mater. Interfaces* **2016**, *8* (24), 15449−15458.

(33) Stewart, I. E.; Ye, S.; Chen, Z.; Flowers, P. F.; Wiley, B. J. Synthesis of Cu−Ag, Cu−Au, and Cu−Pt Core−Shell Nanowires and Their Use in Transparent Conducting Films. *Chem. Mater.* **2015**, *27* (22), 7788−7794.

(34) Wiley, B.; Sun, Y.; Mayers, B.; Xia, Y. Shape-Controlled Synthesis of Metal Nanostructures: The Case of Silver. *Chem. − Eur. J.* **2005**, *11* (2), 454−463.

(35) Mayousse, C.; Celle, C.; Moreau, E.; Mainguet, J.-F.; Carella, A.; Simonato, J.-P. Improvements in Purification of Silver Nanowires by Decantation and Fabrication of Flexible Transparent Electrodes. Application to Capacitive Touch Sensors. *Nanotechnology* **2013**, *24* (21), 215501.

(36) Toybou, D.; Celle, C.; Aude-Garcia, C.; Rabilloud, T.; Simonato, J.-P. A Toxicology-Informed, Safer by Design Approach

for the Fabrication of Transparent Electrodes Based on Silver Nanowires. *Environ. Sci. Nano* **2019**, *6*, 684.

(37) Madeira, A.; Papanastasiou, D. T.; Toupance, T.; Servant, L.; Tréguer-Delapierre, M.; Bellet, D.; Goldthorpe, I. A. Rapid Synthesis of Ultra-Long Silver Nanowires for High Performance Transparent Electrodes. *Nanoscale Adv.* **2020**, *2* (9), 3804−3808.

(38) Sun, Y.; Du, Z. A Flexible and Highly Sensitive Pressure Sensor Based on AgNWs/NRLF for Hand Motion Monitoring. *Nanomaterials* **2019**, *9* (7), 945.

(39) Luan, Y.; Zhang, S.; Nguyen, T. H.; Yang, W.; Noh, J.-S. Polyurethane Sponges Decorated with Reduced Graphene Oxide and Silver Nanowires for Highly Stretchable Gas Sensors. *Sens. Actuators B Chem.* **2018**, *265*, 609−616.

(40) Liu, W.; Li, W.; Yue, L.; Gan, W. Construction of Conductive Three-Dimensional Structure by Low Content of Silver Nanowires and Its Application in Epoxy Resin. *J. Mater. Sci. Mater. Electron.* **2019**, *30* (13), 12307−12314.

(41) Wu, C.; Fang, L.; Huang, X.; Jiang, P. Three-Dimensional Highly Conductive Graphene−Silver Nanowire Hybrid Foams for Flexible and Stretchable Conductors. *ACS Appl. Mater. Interfaces* **2014**, *6* (23), 21026−21034.

(42) Oh, J. Y.; Lee, D.; Hong, S. H. Ice-Templated Bimodal-Porous Silver Nanowire/PDMS Nanocomposites for Stretchable Conductor. *ACS Appl. Mater. Interfaces* **2018**, *10* (25), 21666−21671.

(43) Tian, Z.; Zhao, Y.; Wang, S.; Zhou, G.; Zhao, N.; Wong, C.-P. A Highly Stretchable and Conductive Composite Based on an Emulsion-Templated Silver Nanowire Aerogel. *J. Mater. Chem. A* **2020**, *8* (4), 1724−1730.

(44) Chen, Y.; Zhang, L.; Mei, C.; Li, Y.; Duan, G.; Agarwal, S.; Greiner, A.; Ma, C.; Jiang, S. Wood-Inspired Anisotropic Cellulose Nanofibril Composite Sponges for Multifunctional Applications. *ACS Appl. Mater. Interfaces* **2020**, *12* (31), 35513−35522.

(45) Cheng, R.; Zeng, J.; Wang, B.; Li, J.; Cheng, Z.; Xu, J.; Gao, W.; Chen, K. Ultralight, Flexible and Conductive Silver Nanowire/ Nanofibrillated Cellulose Aerogel for Multifunctional Strain Sensor. *Chem. Eng. J.* **2021**, *424*, 130565.

(46) Zeng, Z.; Chen, M.; Pei, Y.; Seyed Shahabadi, S. I.; Che, B.; Wang, P.; Lu, X. Ultralight and Flexible Polyurethane/Silver Nanowire Nanocomposites with Unidirectional Pores for Highly Effective Electromagnetic Shielding. *ACS Appl. Mater. Interfaces* **2017**, *9* (37), 32211−32219.

(47) Zeng, Z.; Li, W.; Wu, N.; Zhao, S.; Lu, X. Polymer-Assisted Fabrication of Silver Nanowire Cellular Monoliths: Toward Hydrophobic and Ultraflexible High-Performance Electromagnetic Interference Shielding Materials. *ACS Appl. Mater. Interfaces* **2020**, *12* (34), 38584−38592.

(48) Zeng, Z.; Wu, T.; Han, D.; Ren, Q.; Siqueira, G.; Nyström, G. Ultralight, Flexible, and Biomimetic Nanocellulose/Silver Nanowire Aerogels for Electromagnetic Interference Shielding. *ACS Nano* **2020**, *14* (3), 2927−2938.

(49) Romeo, H. E.; Hoppe, C. E.; López-Quintela, M. A.; Williams, R. J. J.; Minaberry, Y.; Jobbágy, M. Directional Freezing of Liquid Crystalline Systems: From Silver Nanowire/PVA Aqueous Dispersions to Highly Ordered and Electrically Conductive Macroporous Scaffolds. *J. Mater. Chem.* **2012**, *22* (18), 9195.

(50) Sannicolo, T.; Lagrange, M.; Cabos, A.; Celle, C.; Simonato, J.-P.; Bellet, D. Metallic Nanowire-Based Transparent Electrodes for Next Generation Flexible Devices: A Review. *Small* **2016**, *12* (44), 6052−6075.

(51) Shen, Y.; Li, D.; Deng, B.; Liu, Q.; Liu, H.; Wu, T. Robust Polyimide Nano/Microfibre Aerogels Welded by Solvent-Vapour for Environmental Applications. *R. Soc. Open Sci.* **2019**, *6* (8), 190596.

(52) Winkler, R.; Ré, E.; Arrachart, G.; Pellet-Rostaing, S. Impact of Solvent Structuring in Water/ *Tert* -Butanol Mixtures on the Assembly of Silica Nanoparticles to Aerogels. *Langmuir* **2019**, *35* (24), 7905−7915.

(53) Liu, M.; Wang, Y.; Ji, J.; Chang, X.; Xu, Q.; Liu, X.; Qin, J. A Facile Method to Fabricate the Polyimide Aerogels with Controllable Microstructure by Freeze-Drying. *Mater. Lett.* **2020**, *267*, 127558.

(54) Deville, S. Ice-Templating, Freeze Casting: Beyond Materials Processing. *J. Mater. Res.* **2013**, *28* (17), 2202−2219.

(55) Kasraian, K.; DeLuca, P. P. Thermal Analysis of the Tertiary Butyl Alcohol-Water System and Its Implications on Freeze-Drying. *Pharm. Res.* **1995**, *12* (4), 484−490.

(56) Orgéas, L.; Dumont, P. J. J.; Vassal, J.-P.; Guiraud, O.; Michaud, V.; Favier, D. In-Plane Conduction of Polymer Composite Plates Reinforced with Architectured Networks of Copper Fibres. *J. Mater. Sci.* **2012**, *47* (6), 2932−2942.

(57) Masse, J. P.; Beyer, K.; Bouvard, D.; Bouaziz, O.; Bréchet, Y.; Salvo, L. Mechanical Behavior of Non Sintered and Sintered Steel Wool. *Adv. Mater. Res.* **2008**, *47−50*, 121−124.

(58) Masse, J. P.; Barbier, C.; Salvo, L.; Bréchet, Y.; Bouaziz, O.; Bouvard, D. Mechanical and Structural Characterization of Non-sintered and Sintered Steel Wools by X-Ray Tomography: Description of the Techniques and Validation on Virtual Materials. *J. Mater. Res.* **2013**, *28* (20), 2852−2860.

(59) Toll, S. Packing Mechanics of Fiber Reinforcements. *Polym. Eng. Sci.* **1998**, *38* (8), 1337−1350.

(60) Masse, J.; Salvo, L.; Rodney, D.; Brechet, Y.; Bouaziz, O. Influence of Relative Density on the Architecture and Mechanical Behaviour of a Steel Metallic Wool. *Scr. Mater.* **2006**, *54* (7), 1379−1383.

(61) Rodney, D.; Gadot, B.; Martinez, O. R.; du Roscoat, S. R.; Orgéas, L. Reversible Dilatancy in Entangled Single-Wire Materials. *Nat. Mater.* **2016**, *15* (1), 72−77.

(62) Gibson, L. J.; Ashby, M. F. *Cellular Solids: Structure and Properties*, 2nd ed.; Cambridge Solid State Science Series; Cambridge University Press: Cambridge, 1997.

(63) Martoïa, F.; Cochereau, T.; Dumont, P. J. J.; Orgéas, L.; Terrien, M.; Belgacem, M. N. Cellulose Nanofibril Foams: Links between Ice-Templating Conditions, Microstructures and Mechanical Properties. *Mater. Des.* **2016**, *104*, 376−391.

(64) Huang, J.; Wang, H.; Liang, B.; Etim, U. J.; Liu, Y.; Li, Y.; Yan, Z. Oriented Freeze-Casting Fabrication of Resilient Copper Nano-wire-Based Aerogel as Robust Piezoresistive Sensor. *Chem. Eng. J.* **2019**, *364*, 28−36.

(65) Yap, L. W.; Gong, S.; Tang, Y.; Zhu, Y.; Cheng, W. Soft Piezoresistive Pressure Sensing Matrix from Copper Nanowires Composite Aerogel. *Sci. Bull.* **2016**, *61* (20), 1624−1630.

(66) Tang, Y.; Gong, S.; Chen, Y.; Yap, L. W.; Cheng, W. Manufacturable Conducting Rubber Ambers and Stretchable Conductors from Copper Nanowire Aerogel Monoliths. *ACS Nano* **2014**, *8* (6), 5707−5714.

(67) Sannicolo, T.; Charvin, N.; Flandin, L.; Kraus, S.; Papanastasiou, D. T.; Celle, C.; Simonato, J.-P.; Muñoz-Rojas, D.; Jiménez, C.; Bellet, D. Electrical Mapping of Silver Nanowire Networks: A Versatile Tool for Imaging Network Homogeneity and Degradation Dynamics during Failure. *ACS Nano* **2018**, *12* (5), 4648−4659.

☐ Recommended by ACS